Influence of Friction Interface Contact on Ultrasonic Motor Efficiency Under Static Conditions

Zhang Yifeng(张毅锋)[1,2*], *Zhang Wu*(张武)[1], *Xiao Aiwu*(肖爱武)[3], *Zhu Meng*(朱萌)[4], *Pan Yunhua*(潘云华)[1], *Zhang Xiaoya*(张小亚)[1]

1. Xi′an Chuang Lian Ultrasonic Technology Co Ltd, Xi′an 710065, P. R. China;
2. School of Marine Science and Tchnology, Northwest Polytechnical University, Xi′an 710065, P. R. China;
3. Xi jing Electronic Corp, Xi′an 710065, P. R. China;
4. Xi′an Modern Control Technology Research Institute, Xi′an 710065, P. R. China

(Received 10 January 2015; revised 26 January 2015; accepted 28 February 2015)

Abstract: The friction interface matching plays a deterministic role in the motor efficiency, and the microcosmic contact status of friction interface should be investigated to improve the ultrasonic motor performance. The main purpose is to improve the effective output power of ultrasonic motor. Hence, one studies the contact condition of the friction interface of the ultrasonic motor, analyzes the micro condition of contact interface through finite element analysis, optimizes unreasonable structures, and compares the two different-structure ultrasonic motors through experiments. The results reflect the necessity of optimization. After optimization, the stator and rotor deform after pre-pressure and the contact interface of them full contact theoretically. When reaching heat balance the effective output of the motor is 37%, and the average effective output efficiency is 2.384 times higher than that of the unoptimized. It can be seen that the total consumption of the ultrasonic motor system decreases significantly. Therefore, when using in certain system the consumption taken from the system will decreases largely, especially in the system with a strict consumption control.

Key words: ultrasonic motor; friction interface; contact area; efficiency

CLC number: TM383 **Document code**: A **Article ID**: 1005-1120(2015)02-0163-11

0 Introduction

Ultrasonic motor is a new concept of micro-special motor, featuring small volume, light weight, compact structure, fast response, low noise and no electro-magnetic interference. As the actuator of a control system, it has a wide application prospect, and has been used in precision positioning field. With high-tech development, the application system has more strict requirements for control accuracy of the movement process. Improving speed stability is necessary for the ultrasonic motor to be widely used in precision control system. Traveling wave type rotary ultrasonic motor(TRUM) (hereinafter referred to as the ultrasonic motor) uses the converse piezoelectric effect of piezoelectric materials to activate vibration of the stator, and turns the micro-amplitude of the stator into rotary movement of the rotor, and exports power[1]. The speed stability of the ultrasonic motor is closely related to the contact interface of the stator and rotor. Kurosawa et al.[2-4] analyzed friction loss between the stator and rotor of the ultrasonic motor in 1988, and theoretically depicted the maximum input and output efficiency of the ultrasonic motor. Wallaschek[5], Zhao et al.[6-7] and Xia et al.[8] qualitatively dissertated that there might be stick-slip on the stator and rotor contact interface, and analyzed the influence of tangential deformation. Storck et al.[9] also studied the influence of the tangential elasticity of the contact on electro-me-

* **Corresponding author**: Zhang Yifeng, Senior Engineer, E-mail: no_bestzhyf@163.com.

How to cite this article: Zhang Yifeng, Zhang Wu, Xiao Aiwu, et al. Influence of friction interface contact on ultrasonic motor efficiency under static conditions[J]. Trans. Nanjing U. Aero. Asrto., 2015,32(2):163-173.
http://dx.doi.org/10.16356/j.1005-1120.2015.02.163

chanical performance of the ultrasonic motor. Maeno et al.[10-11] studied the function of pressure on the friction interface. With consideration of rotor inertia influence on interface, they computed the rotational speed-torque characteristic of the ultrasonic motor and motor performance parameters like energy loss and efficiency. In the condition of contact between flexible stator and rigid rotor, Zharii et al.[12-14] computed the speed and energy conversion efficiency of the ultrasonic motor, and also studied the stator and rotor smooth contact model and stick contact model for the ultrasonic motor. Duan et al.[15] established a complete 3-D model for piezoelectric ceramic and rotor coupling as well as stator and rotor contact interface of the ultrasonic motor. By using finite element software, Zhou et al. established a simplified finite element model which was used to analyze contact of the ultrasonic motor[16], and simulated the influence of pre-pressure and the stator vibration amplitude on output performance of the ultrasonic motor[17]. Radi and Hami[18] conducted the dynamic contact model of stator and rotor contact interface of the ultrasonic motor by variational principle, and used the model into exploring the ineffective model of the ultrasonic motor. However, the above references do not mention the influence of the contact interface on the ultrasonic motor efficiency when the elastic stator and rotor are used under static conditions. Therefore, the structural improvement is presented for current USM-45 ultrasonic motor via redesign of some key parts as well as design of full contact of the stator and rotor contact interface. Some tests have also been conducted. The test results show that, the average output efficiency of improved ultrasonic motor is greatly increased, and the thermal loss rate is decreased by about 30%.

1 Average Effective Output Efficiency of Ultrasonic Motor Property

The average effective output efficiency of the ultrasonic motor is mainly determined by the stator and rotor friction interface and stator structure (mainly elastomer). The stator and rotor of the ultrasonic motor contact directly, they are driven by friction. Generally, alternating voltage is applied on the piezoelectric ceramic element stuck to the stator of the ultrasonic motor, capable of activating mechanical vibration of the stator. The vibration is turned into orientation movement of rotor by the stator and rotor contact friction. Hence, two-energy conversion process exists in the ultrasonic motor. The electro-mechanical energy conversion between the piezoelectric ceramic and stator is fulfilled by converse piezoelectric effect. If the lag effect of the piezoelectric ceramic and elastomer is ignored, the rotor free vibration and electro-mechanical energy conversion of piezoelectric ceramic are linearly reversible. Reversely, electric energy is generated. Based on the above, although the ultrasonic motor is driven by friction, the motor must have greater energy loss. With friction making the motor be heated, the temperature is increasing higher, leading the motor output power to be increasingly smaller. When the ultrasonic motor reaches thermal balance, its effective output power also reaches balance. Therefore, the friction interface matching plays a deterministic role in the motor efficiency, and the microcosmic contact status of friction interface must be studied to improve the ultrasonic motor performance. Curves of torque and rotational speed, and efficiency and torque are as shown in Fig. 1.

In the meantime, the elastomer structure has great effect on effective output efficiency of the ultrasonic motor. Fig. 2 shows a common elastomer structure. A is the total thickness of the elastomer, and B the base thickness of the elastomer.

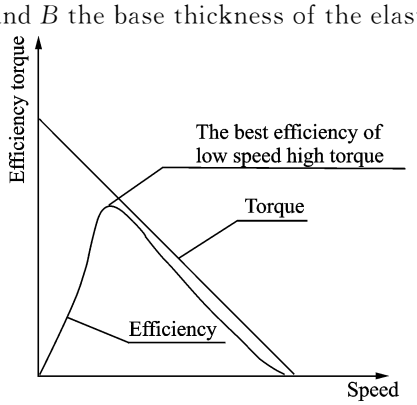

Fig. 1 Curves of torque v. s. rotational speed and efficiency v. s. torque

The base thickness of the elastomer has obvious effect on the dynamics of the stator, directly influencing modal frequency and modal amplitude as well as working current of the motor. The base thickness is bigger, the stator rigidity increases, the same-order modal frequency increases, the working current of the motor increases greatly, the motor heating gradient increases, and the power loss decreases. The base thickness is smaller, the stator rigidity decreases, the same-order modal frequency decreases, the motor output moment decreases while the working current of the motor is decreasing. Therefore, it is not proper to change the elastomer base thickness. If it is required to change, overall evaluation and optimization with more complicated process must be conducted.

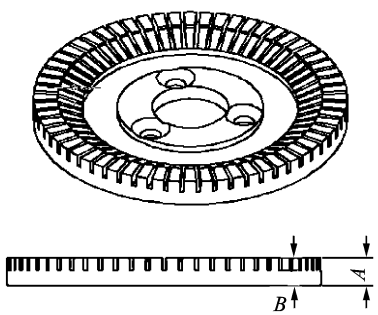

Fig. 2 Elastomer structure

In conclusion, research on the average effective output power of the ultrasonic motor is actually the research on the stator-rotor friction interface contact and rotor base thickness. The paper mainly presents the research on the stator and rotor friction interface contact, optimization design for the stator and rotor friction interface for improvement of the average effective output power of the ultrasonic motor.

2 Stator and Rotor Friction Interface of Ultrasonic Motor Analysis

2.1 Stator and rotor friction interface

The contact model is Hertz contact model. Although stator and rotor contact of the traveling wave ultrasonic motor is not fully the same as general Hertz contact, the Hertz contact theory can better solve the contact friction problem of the traveling wave ultrasonic motor, the torque mathematics model is built.

There are the following hypotheses as per actual working status of the motor:

(1) The materials of the stator and rotor of the traveling wave ultrasonic motor are all elastomer;

(2) The traveling wave surface of the stator and the stator and rotor contact are smooth;

(3) The stator and rotor surfaces are not fully closely contacted;

(4) The stator and rotor of the traveling wave ultrasonic motor do not have relative movement;

(5) The contact of the stator and rotor of the traveling wave ultrasonic motor at the traveling wave peak is curvature cylinder surface contact.

Fig. 3 is the contact model of the iso-curvature radius cylinder and the elatomer plane. It is assumed that, the stator is a iso-curvature radius cylinder at the traveling wave peak, the rotor is a elastic plane, and the rotor contacts the stator within the area with the width of a under pressure action. The contact width a[19-21] is

$$a = 1.6\sqrt{F_N D C_E} \tag{1}$$

where D is the cylinder diameter, F_N the pressure applied on the rotor (at each peak), i. e. pre-pressure, and C_E a parameter related to material characteristic that can be expressed by

$$C_E = \frac{1-\gamma_1^2}{E_1} + \frac{1-\gamma_2^2}{E_2} \tag{2}$$

where E_1 and E_2 are elastic moduli of materials of the stator and rotor, respectively; γ_1 and γ_2 the Poisson ratios of materials of the stator and rotor, respectively.

The locked rotor torque of the motor M[22] is

$$M = \mu_d F_N r \tag{3}$$

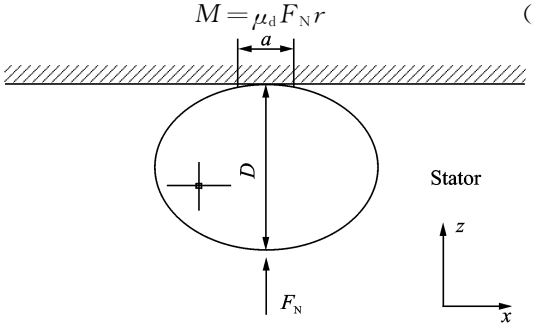

Fig. 3 Hertz contact model

where μ_d is the friction coefficient, and r the average radius of the rotor.

The effective output power of the motor P_{output} is

$$P_{output} = M\omega = M\frac{2\pi n_0}{60} = \mu_d F_N r \frac{2\pi n_0}{60} \quad (4)$$

From Eqs. (1, 3, 4), the relationship between the contact area and effective output power can be obtained

$$P_{output} = \mu_d \frac{2\pi n_0 r a^2}{96DC_E} = \mu_d \frac{\pi n_0 r a^2}{48D\left(\frac{1-\gamma_1^2}{E_1} + \frac{1-\gamma_2^2}{E_2}\right)} \quad (5)$$

The variables in Eq. (5) are n_0 and a, the other paramenters can be marked as constant Z

$$Z = \frac{\mu_d \pi r}{48D\left(\frac{1-\gamma_1^2}{E_1} + \frac{1-\gamma_2^2}{E_2}\right)} \quad (6)$$

Then Eq. (5) can be simplified as

$$P_{output} = Zn_0 a^2 \quad (7)$$

From Eq. (7), we can obtain the conclusion that, when the rotating speed of the motor is not changed, the output power of the motor is directly proportional to the square of the stator and rotor contact width. The wider the contact width is, the bigger the contact area is, and vice versa.

2.2 Stator and rotor contact model of ultrasonic motor

The structure of the traveling wave ultrasonic motor is shown in Fig. 4. Firstly, the elastomer is fixed on the motor base, then the rotor is placed on the elastomer, the circular disk at the rotor center is used to apply pre-pressure. To make the traveling wave ultrasonic motor output great moment, great axial pre-pressure is usually applied between the stator and rotor. In the mean time, the pre-pressure can make the stator and rotor bend in radial.

It is found that, because of radial bending, the actual stator and rotor contact area decreases greatly, and pressure is not evenly distributed. The stator and rotor contact is rapidly worn and heat loss power is sharply increased, leading to very low ultrasonic motor efficiency, as shown in Fig. 5.

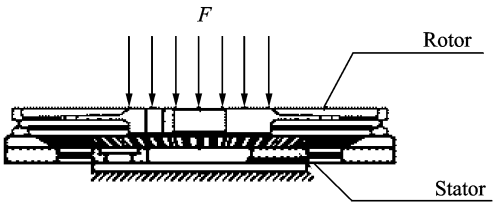

Fig. 4 Stator and rotor coordination section of ultrasonic motor

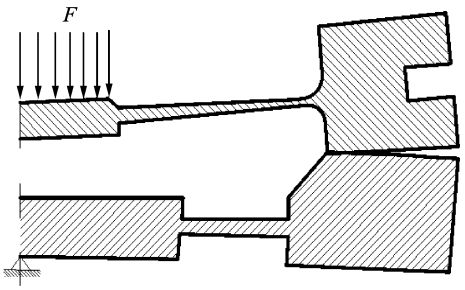

Fig. 5 Stator and rotor radial bending effect

2.3 Simulation analysis

2.3.1 Building finite element model

The finite element model is built by means of ABAQUS[23]. Since the rotor and stator model is equally divided into three parts along the circumference, the finite element model is only for the 1/3 part of the model (Fig. 6). In the model, the inner circular ring at the base of the stator is taken as the rigid body, the Kulun friction coeficient of the stator and rotor is 0.2, the prepressure is 160 N, i.e. about 1 MPa pressure intensity is applied onto the disk at the rotor center.

2.3.2 Model analysis

The whole analysis result is shown in Fig. 7. In Fig. 7, it is found that, the displacement of the rotor outer edge is up (positive value), and the displacement of the stator outer edge is down (negative value), at this time, there is gap at the contact between the stator outer edge and rotor outer edge. That is, the stator and rotor contact width is not the whole rotor contact surface, is a part of the rotor contact surface. Check the displacement diagrams respectively, as shown in Figs. 8, 9. In the diagrams, XIA-1 is the simulation data of the stator, and SHANG-1 the simula-

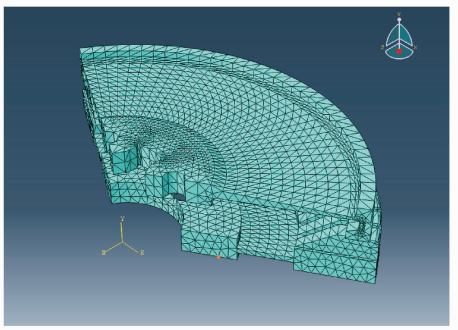

Fig. 6 Finite element analysis model of USM45 ultrasonic motor

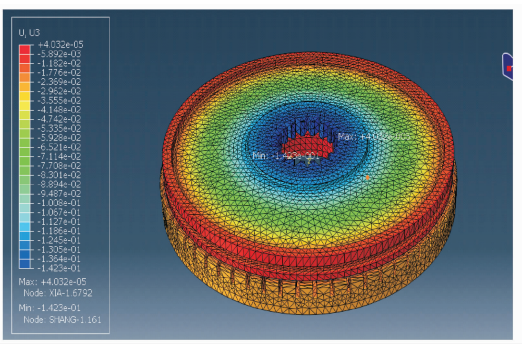

Fig. 7 USM45 stator finite element analysis of displacement

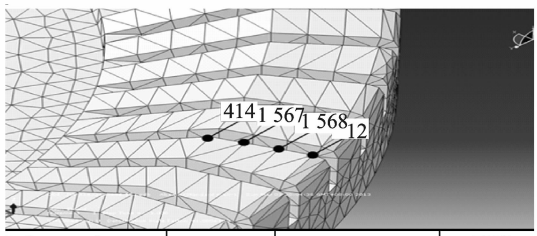

Nodes part instance	Node ID	Attached element	U,U_3
XIA-1	414	7 828	−0.017
XIA-1	1 567	7 948	−0.018
XIA-1	1 568	11 595	−0.021
XIA-1	12	21 417	−0.023

Fig. 8 Stator displacement before optimization

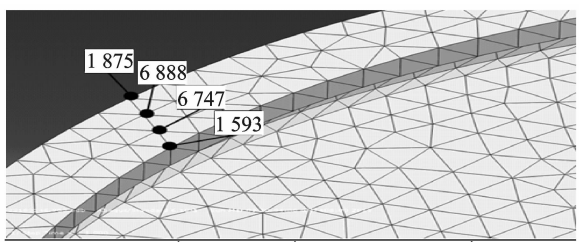

Part instance	Node ID	Attached element	U,U_3
SHANG-1	1 593	27 020	−0.017
SHANG-1	6 747	5 025	−0.016
SHANG-1	6 888	6 264	−0.013
SHANG-1	1 875	2 461	−0.010

Fig. 9 Rotor displacement before optimization

tion data of the rotor. Draw the curvesby the data, as shown in Fig. 10. It is shown that, the 2 mm length of rotor radial contact is actually inner 0.3 mm contact with an area of 42.96 mm^2, and outer ring width is 1.7 mm, being separated, with an area of 252.61 mm^2. The contact acreage of the stator and rotor is only 14.5% of the theoretical contact acreage, which makes the pressure of the contact acreage too high and increases the inner cycling stress of the friction materials, and finally makes rapid wear of the friction materials and heat of the moter. At this time, the heat energy loss of the motor is increased to 3 times as much as the theoretical heat energy loss, making the effective output power of the motor decreases greatly.

2.4 Structure optimization

The data shown in Fig. 10 are the reference for the stator and rotor structure optimization. The optimization idea is to make the two curves in Fig. 10 approach to coincide. Where s is the displacement. Therefore, deformation displacements of the stator and rotor are approximately the same, and the actual contact area is close to the theoretical contact area. According to the data analysis in Table 1, after deformation, the displacement of the inner rotor is 0.001 968 mm more than that of the inner stator, and the displacement of the outer rotor is 0.012 071 3 mm

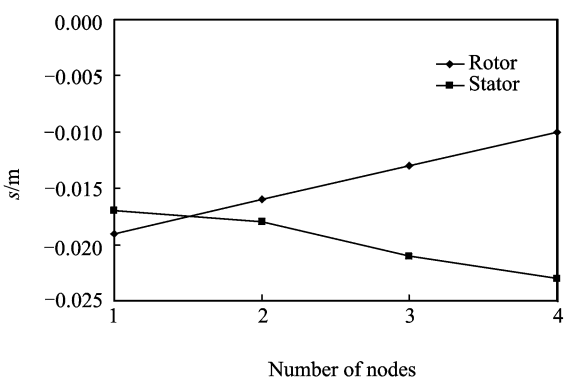

Fig. 10 Displacements of stator and rotor contacting ring surface in pre-pressure status

Table 1 Displacement data of stator and rotor contacting ring surface in pre-pressure status

Nodes	Displacement/mm	Displacement difference/mm
414(Rotor)	−0.017	0.000
1 593(Stator)	−0.017	
1 567(Rotor)	−0.016	0.002
6 747(Stator)	−0.018	
1 568(Rotor)	−0.013	0.008
6 888(Stator)	−0.021	
12(Rotor)	−0.010	0.013
1 875(Stator)	−0.023	

less than that of the outer elastomer. The inner displacement difference value is only 1/6 of the outer one. The optimization neglects the inner displacement difference value, focusing on the outer displacement difference value.

In new structure, with consideration of the friction surface of the rotor being stuck with friction slice, so only the stator structure is optimized. The original design is that the friction surface of the stator is a parallel surface. Now the friction surface of the stator is designed into a conical surface with an outside displacement difference from the inner to the outer, to counteract the outer displacement difference while the stator and rotor deforming. The converted angle is about 0.2°. Therefore, in elatomer structure design, the tooth surface of the elatomer is designed as taper and the conical degree is 0.2°, which makes the two curves shown in Fig. 7 approach to coincide, structure before and after contrast is shown in Fig. 11.

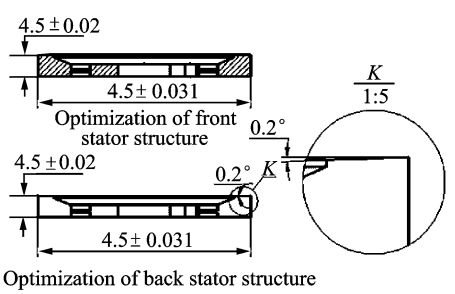

Fig. 11 Stator structure

Draw a 3-D mathematic model again as per the optimized structure, and analysis by ABAQUS. The friction coefficient and pre-pressure are set the same as those before optimization. The analysis results are shown in Figs. 12, 13. XIA-1 is the stator simulation data, SHANG-1 is the rotor simulation data. Concrete analysis data are shown in Table 2. Draw the curves by means of the analysis data of Table 2, as shown in Fig. 14. It is found that, the deformation amount of the rotor is basic the same from the inner ring contacting to the outer ring contacting, and the changing magnitude is 10—14 mm, which can be neglected during actual machining and grinding. According to the displacement data of the rotor contacting the ring surface, it is found that the down displacement of the outer ring is more than that of the inner ring. It is obtained by calculation that, the deformation angle for ring surface contacting is about 0.194°, which approaches to the converted angle in stator optimization design, i.e. the contact surface of stator is approximately parallel to the fixed bottom after stator deformation. Additionally, on the basis of the deformation data in Fig. 14, it is found that, the deformation displacement values of the nodes corresponding to the inner stator and rotor of the ring surface of the contract circle are -5.43×10^{-2} and -5.66×10^{-2}, respectively, the difference is 1.7 μm. The nodes can be considered as deformation coincidence.

Table 2 Displacement data of stator and rotor contacting ring surface in pre-pressure status after optimization

Nodes	Displacement/mm	Displacement difference/mm
414(Rotor)	−0.019	−0.002
1 593(Stator)	−0.017	
1 567(Rotor)	−0.019	−0.001
6 747(Stator)	−0.018	
1 568(Rotor)	−0.019	0.000
6 888(Stator)	−0.019	
12(Rotor)	−0.020	0.003
1 875(Stator)	−0.023	

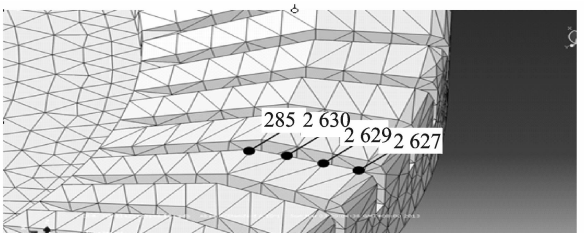

Nodes part instance	Node ID	Attached element	U,U_3
XIA-1	285	7 145	−0.017
XIA-1	2 630	954	−0.018
XIA-1	2 629	1 037	−0.019
XIA-1	2 627	30 244	−0.023

Fig. 12 Stator displacement after optimization

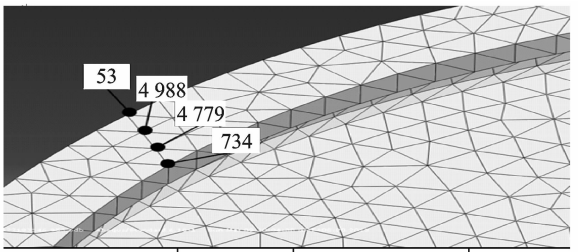

Nodes part instance	Node ID	Attached element	U,U_3
SHANG-1	734	16 765	−0.019
SHANG-1	4 779	17 728	−0.019
SHANG-1	4 988	15 517	−0.019
SHANG-1	53	6 688	−0.020

Fig. 13 Rotor displacement after optimization

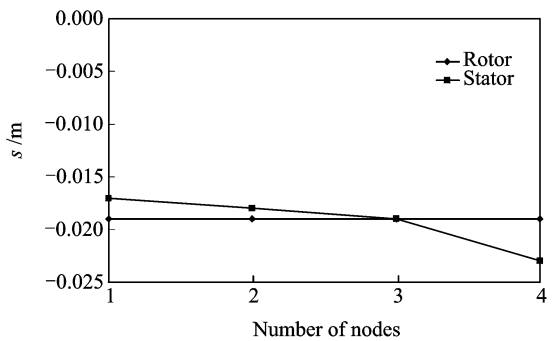

Fig. 14 Displacements of stator and rotor contacting ring surface in pre-pressure status after optimization

Therefore, it is concluded that, after optimization, when the stator and rotor are deformed in pre-pressure status, the stator and rotor contact surface fully contacts in a theoretical manner.

3 Experiment

3.1 Experimental facilities

Magtrol power analyzer is used, including electric analyzer and motor test system. Electric analyzer includes Dynamom Etermodel: DSP6001 and Power analyzer model: 6510S (Figs. 15, 16).

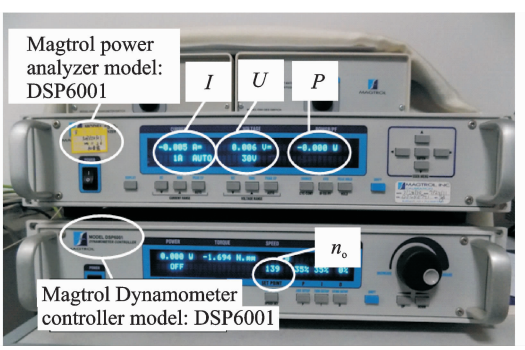

Fig. 15 Electric analyzer

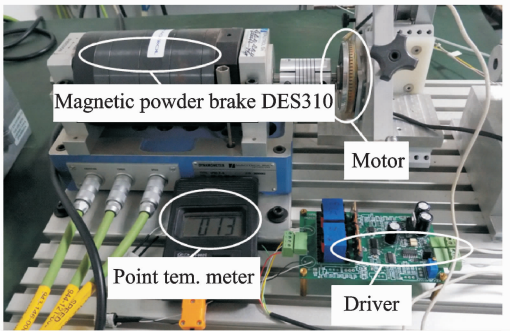

Fig. 16 Motor test system

3.2 Experimental law

Conduct machining as per the optimized stator, and assemble into a motor to do the performance experiment. The experimental law is as follows:

Set the input voltage as $U=24$ V, the environmental temperature 21 ℃, the start rotating speed $\tau=115$ r/min, and the start pre-pressure 0.5 N·m, the experimental law is tested once every 5 min. The data to be tested include current I, rotating speed r, temperature t, and locked rotor torque M. Moreover, test the data for two-structure motors before and after optimization, and test the data for one-hour motor running. There are 13 groups of data in total, as shown in Tables 3, 4, respectively.

Table 3 Motor test data before optimization

Times	$r/(\mathrm{r\cdot min^{-1}})$	$M/(\mathrm{N\cdot m})$	$t/℃$	I/A
1	105.00	0.24	32.00	0.49
2	94.20	0.24	53.00	0.49
3	88.00	0.26	62.00	0.52
4	84.50	0.26	70.00	0.53
5	80.50	0.26	74.00	0.53
6	78.40	0.26	78.00	0.54
7	81.50	0.26	78.00	0.55
8	78.50	0.26	78.50	0.55
9	76.00	0.26	80.00	0.54
10	74.20	0.26	81.00	0.55
11	73.00	0.26	82.00	0.55
12	73.60	0.26	82.00	0.55
13	73.20	0.26	82.00	0.55

3.3 Result analysis

3.3.1 Basic curve analysis

It is shown in Tables 3, 4 that, the temperature at which the motor reaches heat balance be-

Table 4 Motor test data after optimization

Times	$r/(\mathrm{r}\cdot\mathrm{min}^{-1})$	$M/(\mathrm{N}\cdot\mathrm{m})$	$t/℃$	I/A
1	105.00	0.38	24.00	0.31
2	102.00	0.38	34.00	0.3
3	95.60	0.34	38.00	0.31
4	91.00	0.36	44.00	0.30
5	83.20	0.32	51.00	0.29
6	80.00	0.34	53.00	0.31
7	78.00	0.34	55.00	0.31
8	78.00	0.32	55.00	0.31
9	77.20	0.34	57.00	0.31
10	77.00	0.34	57.00	0.31
11	77.50	0.34	57.00	0.31
12	78.00	0.34	57.00	0.31
13	80.00	0.34	57.00	0.32

fore optimization is 80 ℃, and is 57 ℃ after optimization. Before optimization, the null running current of the motor for each test is average 1.6 times as much as the post-optimization one. After optimization, the locked rotor torque of the motor for each test is average 1.5 times as much as the pre-optimization one. Because the locked rotor torque M and the current I are percentile data, when draw curves as per the data in Tables 3, 4, the locked rotor torque M and the current I are magnified 100 times, the tested 4 types of parameters can be used for drawing in a same curve graph, as shown in Figs. 17, 18.

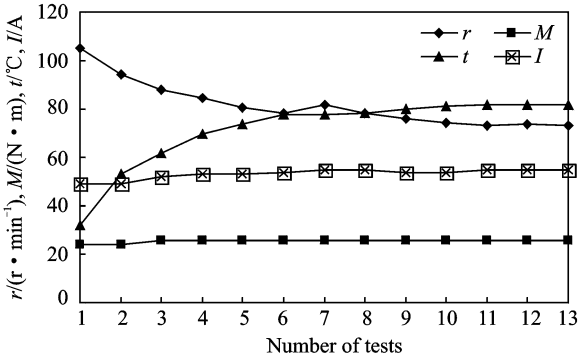

Fig. 17 Pre-optimization motor parameter-time

3.3.2 Ultrasonic motor efficiency analysis

The total power consumption of the ultrasonic motor consists of the power consumption of the motor-driven controller and the power consumption of the motor. The motor power consumption includes the motor effective output power consumption and the motor heating power consumption

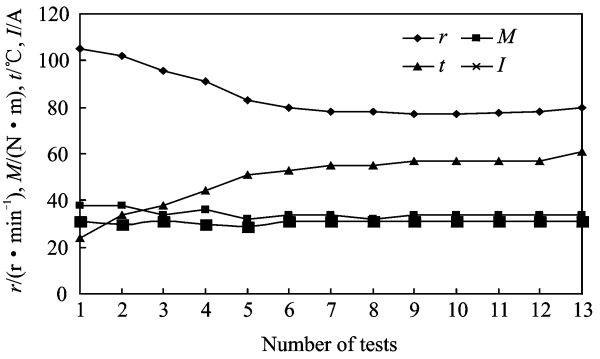

Fig. 18 Post-optimization motor parameter-time

$$P_{\mathrm{total}} = P_{\mathrm{motor}} + P_{\mathrm{drive}} \tag{8}$$

$$P_{\mathrm{total}} = P_{\mathrm{output}} + P_{\mathrm{heat}} + P_{\mathrm{drive}} \tag{9}$$

In test, the input voltage of the motor is 24 V, the motor current changes with time. The solvable motor power changing with time is the total power consumption of the motor. There are two calculation schemes for the power consumption of the ultrasonic motor-driven controller. The first is adding power consumption of each element / device. The second one is testing the controlling circuit board bus over current of the ultrasonic motor driver in the case of voltage for the fixed value, and then multiplying the current by the voltage. Here, the second scheme is adopted, the tested overcurrent of the circuit board is 5 mA, then the power consumption of the driver circuit board is

$$P_{\mathrm{drive}} = U \times I_{\mathrm{drive}} = 24 \times 0.005\ \mathrm{W} = 0.12\ \mathrm{W} \tag{10}$$

The output power of the ultrasonic motor is

$$P_{\mathrm{output}} = M\omega = M\frac{2\pi n_0}{60} \approx 0.104\ 7Mn_0 \tag{11}$$

where M is the locked rotor torque of the motor, ω the no-load angular speed of the motor, and n_0 the on-load rotating speed of the motor.

The effective output power of the motor is

$$\eta = \frac{P_{\mathrm{output}}}{P_{\mathrm{total}}} \tag{12}$$

The P_{total}, P_{motor}, P_{drive}, P_{heat} and η can be calculated by Eqs. (8—12).

According to Tables 3, 4, calculate corresponding parameters shown in Tables 5, 6. Then

draw each power curve as per Tables 5, 6, as shown in Figs. 19, 20. After optimization, the efficiency comparison result is shown in Fig. 21. It is known that, before optimization, the highest effective output efficiency of the motor is only 0.224, when heat balance is reached, the effective output efficiency of the motor is only 0.151, and the average effective output efficiency is 0.172, and the loss efficiency by motor heating rises to 0.84 after heat balance from the start 0.765. After optimization, the effective output efficiency of the motor is increased greatly with the highest value of 0.561, and it is about 0.37 after heat balance, the average output efficiency is 0.41. Meanwhile, the motor heating loss efficiency is decreased greatly, rising to 0.613 from 0.422 with the average value of 0.575. Additionally, it is also found that, the total power of the motor decreases greatly. The total power of the motor before optimization is 12.8 W in average, and it is only 7.38 W after optimization. That is to say, when the ultrasonic motor is used in a system, the power consumption of a whole system decreases greatly, being very important for application in a system with strict control for power consumption.

Table 5 Power and efficiency of motor before optimization

Times	P_{motor}	P_{total}	P_{drive}	P_{heat}	η
1	2.64	11.76	0.12	9.00	0.22
2	2.37	11.76	0.12	9.27	0.20
3	2.39	12.48	0.12	9.96	0.19
4	2.30	12.72	0.12	10.30	0.18
5	2.19	12.72	0.12	10.41	0.17
6	2.13	12.96	0.12	10.71	0.16
7	2.22	13.20	0.12	10.86	0.16
8	2.14	13.20	0.12	10.94	0.16
9	2.07	12.96	0.12	10.77	0.15
10	2.02	12.96	0.12	10.82	0.15
11	1.99	13.20	0.12	11.09	0.15
12	2.00	13.20	0.12	11.08	0.15
13	1.99	13.20	0.12	11.09	0.15

Table 6 Power and efficiency of motor after optimization

Times	P_{motor}	P_{total}	P_{drive}	P_{heat}	η
1	4.18	7.44	0.12	3.14	0.56
2	3.59	7.20	0.12	3.49	0.50
3	3.40	7.44	0.12	3.92	0.46
4	3.11	7.20	0.12	3.97	0.43
5	2.79	6.96	0.12	4.05	0.40
6	2.85	9.44	0.12	4.47	0.30
7	2.78	7.44	0.12	4.54	0.37
8	2.61	7.44	0.12	4.71	0.35
9	2.75	7.44	0.12	4.57	0.37
10	2.74	7.44	0.12	4.59	0.37
11	2.76	7.44	0.12	4.56	0.37
12	2.77	7.44	0.12	4.54	0.37
13	2.85	7.68	0.12	4.71	0.37

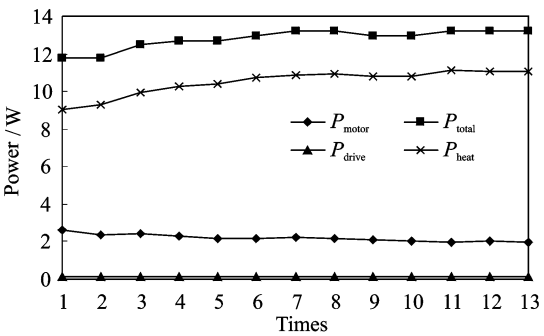

Fig. 19 Motor power before optimization

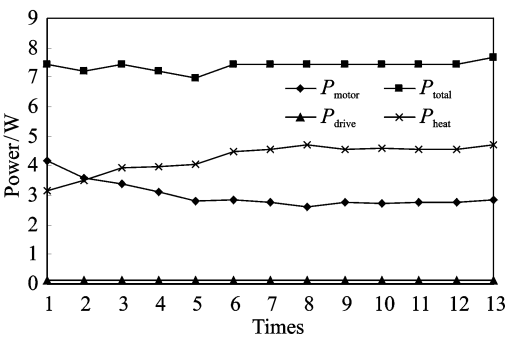

Fig. 20 Motor power after optimization

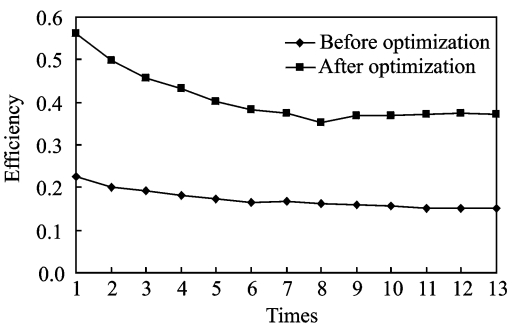

Fig. 21 Motor efficiency before and after optimization

4 Conclusions

Before optimization, the contact area of stator and rotor is only 14.5% of theoretical area, and it makes the pressure of contact area too big

and enlarges the inner stress of friction material which makes rapid wear of it and heat of the motor, at last the effective output power of the motor is only 17%. After optimization, the stator and rotor deform after pre-pressure and the contact interface of both approaches theoretically full contact. When reaching heat balance the effective output of the motor is 37%, and the average effective output efficiency is 2.384 times compared with the one which has not been optimized.

Meanwhile, the heat loss of motor deceases greatly, which comes from 10.48 W before optimization to 4.31 W after optimization, and according to the total power, the efficiency of heat loss decreases 30% after optimization. Moreover, the motor total power decreases greatly, which comes from 12.8 W the average before optimization to 7.38 W after it and is 58% of the one before optimization. It can be seen that the total consumption of the ultrasonic motor system decreases greatly, in other words, when using in certain system, the consumption will decreases greatly, especially in the system which has strict consumption control.

References:

[1] Zhao Chunsheng. Ultrasonic motors technologies and applications[M]. Beijing: Science Press, 2007.

[2] Minoru Kurosawa, Kentaro Nakamura, Takashi Okamoto, et al. An ultrasonic motor using bending vibration of a short cylinder[J]. IEEE Transactions on Ultrasonic, Ferroelectrics and Frequency Control, 1989, 36(5): 517-521.

[3] Minoru Kurosawa, Kentaro Nakamura, Sadayuki Ueha. Numerical analysis of the property of a hybird transducer type ultrasonic motor[C]// IEEE Proceeding of Ultrasonic Symposium. [S. l.]: IEEE, 1990: 1187-1190.

[4] Minoru Kurosawa, Tatsuya Uchiki, Hideto Hanada, et al. Simulation and experimental study on elastic FIN ultrasonicmotor[C]// IEEE Proceeding of Ultrasonic Symposium. [S. l.]: IEEE, 1992: 893-896.

[5] Wallaschek J. Contact mechanics of piezoelectrical trasonic motors[J]. Smart Materials & Structures, 1998, 7(5): 369-381.

[6] Zhao Xiangdong. Study on the dynamic modeling and simulation of the traveling wave type ultrasonic motor [D]. Nanjing: Nanjing University of Aeronautics and Astronautics, 2000. (in Chinese)

[7] Zhao Xiangdong, Chen Bo, Zhao Chunsheng. Nonlinearly frictional interface model of rotated traveling wave type ultrasonic motor[J]. Journal of Nanjing University of Aeronautics & Astronautic, 2003, 35(6): 629-633. (in Chinese)

[8] Xia Changliang, Zheng Yao, Shi Tingna, et al. FEM analysis on stator vibration of traveling wave type contact ultrasonic motor [J]. Proceedings of the CSEE, 2002, 21(2): 25-28. (in Chinese)

[9] Storck H, Wallaschek J. The effect of tangential elasticity of the contact layer between stator and rotor in travelling wave ultrasonic motors[J]. International Journal of Non-Linear Mechanics, 2003, 38(2): 143-159.

[10] Takashi Maeno, Bogy David B. Effect of the hydrodynamic bearing on rotor/stator contact in a ring-type ultrasonic motor[J]. IEEE Transactions on Ultrasonic Ferroelectric Frequency Control, 1992, 39(6): 675-682.

[11] Takashi Maeno, Takayuki Tsukimoto, Akira Miyake. Finite-element analysis of the rotor/stator contact in a ring-type ultrasonic motor[J]. IEEE Transactions on Ultrasonic Ferroelectric Frequency Control, 1992, 39(6): 668-674.

[12] Zharii O Y. Modeling of a mode conversion ultrasonic motor in the regime of slip[J]. IEEE Transactions on Ultrasonic Ferroelectric Frequency Control, 1993, 40(4): 411-417.

[13] Zharii O Y. Adhesive contact between the running Rayleigh wave and a rigid strip[J]. Transactions of the ASME, Journal of Applied Mechanicas, 1995, 62: 368-372.

[14] Zharii O Y, Ulitko A F. Smooth contact between the running Rayleigh wave and a rigid strip[J]. Transactions of the ASME, Journal of Applied Mechanicas, 1995, 62: 362-367.

[15] Duan W H, Quek S T, Lim S P. Finite element solution for intermittent-contact problem with piezoelectric actuation in ring type USM[J]. Finite Elements in Analysis and Design, 2007, 43(3): 193-205.

[16] Zhou Shengqiang, Zhao Chunsheng. Two simplified finite element models for contact analysis of ultrasonicmotor[J]. Journal of Vibration, Measurement &

Diagnosis, 2009, 29(3): 251-255. (in Chinese)

[17] Zhou Shengqiang, Zhao Chunsheng, Huang Weiqing. Contact analysis of traveling wave type rotary ultrasonic motor in space domain[J]. Proceedings of the CSEE, 2010, 30(12): 63-68. (in Chinese)

[18] Radi B, Hami A E I. The study of the dynamic contact in ultrasonic motor[J]. Applied Mathematical Modeling, 2010, 34(12): 3767-3777.

[19] Young W C. Roark's formulas for stress and strain [M]. New York: Mc Graw-Hill, 2011.

[20] Ding Huolin. Principles of tribology[M]. Beijing: China Machine Press, 1981.

[21] Wen Shizhu. Principles of tribology[M]. Beijing: Tsinghua University Press, 1990.

[22] Hu Minqiang, Jin Long, Gu Juping. Ultrasonic motor principles and design[M]. Beijing: Science Press, 2005.

[23] Shi Yiping, Zhou Yurong. The ABAQUS finite element analysis example[M]. Beijing: China Machine Press, 2006.

(Executive editor: Xu Chengting)